Research in Astron. Astrophys. **2009** Vol. **9** No. **12**, 1343–1350
http://www.raa-journal.org *http://www.iop.org/journals/raa*

***R**esearch in*
***A**stronomy and*
***A**strophysics*

A multiwavelength study of the massive star-forming region IRAS 22506+5944 *

Yuan-Wei Wu[1], Ye Xu[1], Ji Yang[1] and Jing-Jing Li[2]

[1] Purple Mountain Observatory, Chinese Academy of Sciences, Nanjing 210008, China; *ywwu@pmo.ac.cn*
[2] Shanghai Observatory, Chinese Academy of Sciences, Shanghai 200030, China

Received 2009 February 6; accepted 2009 September 22

Abstract We present a multi-line study of the massive star-forming region IRAS 22506+5944. A new 6.7 GHz methanol maser was detected. ^{12}CO, ^{13}CO, C^{18}O and HCO$^+$ $J = 1 - 0$ transition observations reveal a star-formation complex consisting mainly of two cores. The dominant core has a mass of more than 200 $M_\odot$, while the other one is only about 35 $M_\odot$. Both cores are obviously at different evolutionary stages. A ^{12}CO energetic bipolar outflow was detected with an outflow mass of about 15 $M_\odot$.

Key words: infrared: ISM — ISM: individual (IRAS 22506+5944) — ISM: jets and outflows — masers — stars: formation

1 INTRODUCTION

Massive stars play an important role in the evolution of the interstellar medium (ISM) and galaxies; nevertheless, their formation process is still poorly understood because of large distances, high extinctions, and short timescales of critical evolutionary phases. In addition, massive stars do not form in isolation but rather are often in clusters and associations, which makes the environment of massive star formation regions more complex.

The 6.7 GHz transition of methanol has been found to be a particularly useful signpost to trace massive star formation (Minier et al. 2003; Xu et al. 2003). On the other hand, the maser phase encompasses the outflow phase (Xu et al. 2006), which gives us another powerful tool to study the dynamics of massive star formations.

IRAS 22506+5944, with an infrared luminosity of $1.5\times10^4 L_\odot$, belongs to the Cepheus molecular cloud complex. Harju et al. (1993) made an NH_3 map of this region, and found that an NH_3 core coincides with the peak of the IRAS source. Both an H_2O maser (Wouterloot & Walmsley 1986) and SiO (Harju et al. 1998) have been detected. Although searches for a 6.7 GHz methanol maser (Szymczak et al. 2000) show negative results, we recently found a weak 6.7 GHz methanol maser in this region. Despite the high luminosity and FIR color characteristics of the ultra-compact HII region, no radio emission was detected (Molinari et al. 1998). The distances used in the literatures for this source range from 5.0 kpc to 5.7 kpc. Here, we use a value of 5.0 kpc.

In this paper, we present a multi-line study of this star-forming region. In Section 2, we describe our observations. The results are given in Section 3. We give an analysis and discussion in Section 4, and we summarize in Section 5.

* Supported by the National Natural Science Foundation of China.

2 OBSERVATIONS

2.1 The Effelsberg 100 m Telescope

Observations of the methanol (CH_3OH) maser were made using the Effelsberg 100 m telescope in 2006 February. The rest frequency adopted for the $5_1 - 6_0$ A^+ transition was 6668.519 MHz (Breckenridge & Kukolich 1995). The spectrometer was configured to have a 10 MHz bandwidth with 4096 channels yielding a spectral resolution of 0.11 km s^{-1} and a velocity coverage of 450 km s^{-1}. The half-power beam width was $\sim 2'$ and the telescope had an rms pointing error of $10''$. The observations were made in position switched mode. The system temperature was typically around 35 K during our observations. The flux density scale was determined by observations of NGC 7027 (Ott et al. 1994). The absolute calibration for flux density is estimated to be accurate to $\sim 10\%$. The integration time on the source was 10 min, with an rms noise level of ~ 0.05 Jy in the spectra. The pointing position was R.A.(J2000) $22^h52^m36.9^s$, DEC.(J2000) = $+60°00'48''$.

2.2 The PMO 13.7 m Telescope at Delingha

The ^{12}CO, ^{13}CO, $C^{18}O$ and HCO^+ $J = 1 - 0$ maps were observed with the PMO 13.7 m millimeter-wave telescope at Delingha, China, during 2008 November. A cooled SIS receiver was employed, and the system temperature was ~ 250 K during the observations. Three AOS (acousto-optical spectrometers) were used to measure the $J = 1 - 0$ transitions of ^{12}CO, ^{13}CO, $C^{18}O$ and an FFTS (Fast Fourier Transform Spectrometer) was used to measure the HCO^+ $J = 1 - 0$ lines. All the observations were performed in position switch mode. The pointing and tracking accuracy was better than $10''$. The obtained spectra were calibrated in the scale of antenna temperature T_A^* during the observation and corrected for atmospheric and ohmic loss by the standard chopper wheel method. The grid spacings of the mapping observations were $30''$. Table 1 summarizes the basic information about our observations, including: the transitions, the center rest frequencies $\nu_{\rm rest}$, the half-power beam widths (HPBWs), the bandwidths, the equivalent velocity resolutions ($\Delta\nu_{\rm res}$), and the typical rms levels of measured spectra. All of the spectral data were transformed from the T_A^* to the main beam brightness temperature T_{MB}^* scale. The absolute calibration for intensity was about 10%.

The GILDAS software package (CLASS & GREG) was used for the data reduction.

Table 1 Observation Parameters

Translation	$\nu_{\rm rest}$ (GHz)	HPBW ($''$)	Bandwidth (MHz)	$\Delta\nu_{\rm res}$ (km s^{-1})	1σ rsm[a] (K)
^{12}CO $J = 1 - 0$	115.271204	58	145	0.37	0.10
^{13}CO $J = 1 - 0$	110.201353	61	43	0.11	0.10
$C^{18}O$ $J = 1 - 0$	109.782182	62	43	0.12	0.09
HCO^+ $J = 1 - 0$	89.188521	75	43	0.16	0.10

[a] Typical values in the scale of T_R^*.

3 RESULTS AND DISCUSSION

3.1 Spectra

3.1.1 6.7 GHz CH_3OH *maser spectrum*

The spectrum of the CH_3OH maser detected in this region is shown in Figure 1. There are two features that are separated by about 2.2 km s^{-1}. The stronger feature is at the LSR (local standard of rest) velocity of –53.7 km s^{-1}, with a flux density of 0.52 Jy, while the other is only about 0.2 Jy. In order to get high signal to noise spectra, we did not attempt to refine the position and just integrated the time at the same position. Hence, the actual position could be off by 1 arcmin.

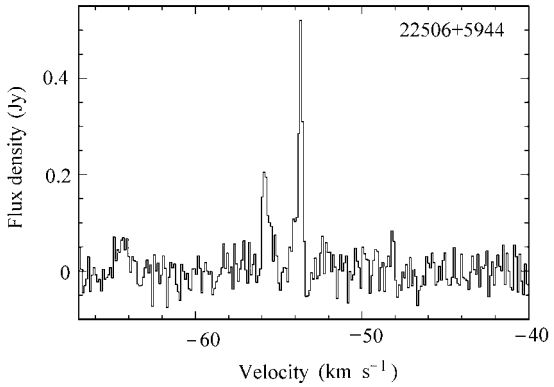

Fig. 1 Spectrum of the 6.7-GHz CH_3OH maser. The spectral resolution is 0.11 km s^{-1}.

3.1.2 ^{12}CO, ^{13}CO, C^{18}O *and* HCO$^+$ *spectra*

Spectra of ^{12}CO, ^{13}CO, C^{18}O and HCO$^+$ are presented in Figure 2. The spectra in the left panel come from the peak of Core A (dominant core in Fig. 3). Both ^{12}CO and HCO$^+$ show remarkable broad line wings, with an FW (full width) of 24 km s^{-1} and 6 km s^{-1} at the 1σ level, respectively. Spectra in the right panel correspond to the peak of Core B, and spectra at the conjunctive point of the two cores are given in the middle panel. Spectral parameters of Cores A and B (peak position), including line central velocities, fitted line widths, bright temperatures and integrated intensities, are listed in Table 2.

Table 2 Result of Molecular Line Measurements

Translation (GHz)	$V_{\rm LSR}$ (km s^{-1})	$\Delta v_{\rm res}$ (km s^{-1})	$T^*_{\rm MB}$ (K)	$\int T^*_{\rm MB}\, dv$ (K km s^{-1})
^{12}CO $J = 1-0$ [a]	–51.4	4.3	22.3	98.3
^{12}CO $J = 1-0$ [b]	–51.5	3.3	14.1	48.9
^{13}CO $J = 1-0$ [a]	–51.4	2.3	9.5	22.1
^{13}CO $J = 1-0$ [b]	–51.5	1.8	6.1	11.4
C^{18}O $J = 1-0$ [a]	–51.6	1.8	1.2	2.3
C^{18}O $J = 1-0$ [b]	–51.5	1.1	0.9	1.0
HCO$^+$ $J = 1-0$ [a]	–51.1	3.8	2.1	6.9
HCO$^+$ $J = 1-0$ [b]	–51.6	2.0	0.4	0.9

[a] and [b] indicate Core A and Core B.

3.2 Mapping

3.2.1 ^{13}CO, C^{18}O *and* HCO$^+$ *maps*

Contour maps of the total integrated ^{13}CO $J = 1-0$, C^{18}O $J = 1-0$ and HCO$^+$ $J = 1-0$ line emissions are presented in Figure 3. We used an MSX E band (21 μm) image as the background image for the integrated contours to compare the distributions of gas and dust. The filled triangle denotes the 3 millimeter continuum peak (Su et al. 2004). H_2O (Wooterloot & Walmsley 1986), SiO (Harju et al. 1998) and CH_3OH masers are indicated by the open triangle, star and square, respectively. The IRAS error ellipse is also marked. Contour levels are 20% to 90% in steps of 10% of the peak emission with the exception of the HCO$^+$ $J = 1-0$ line, whose contour levels are 10%, 15% and 20% to 90% in steps of 10%.

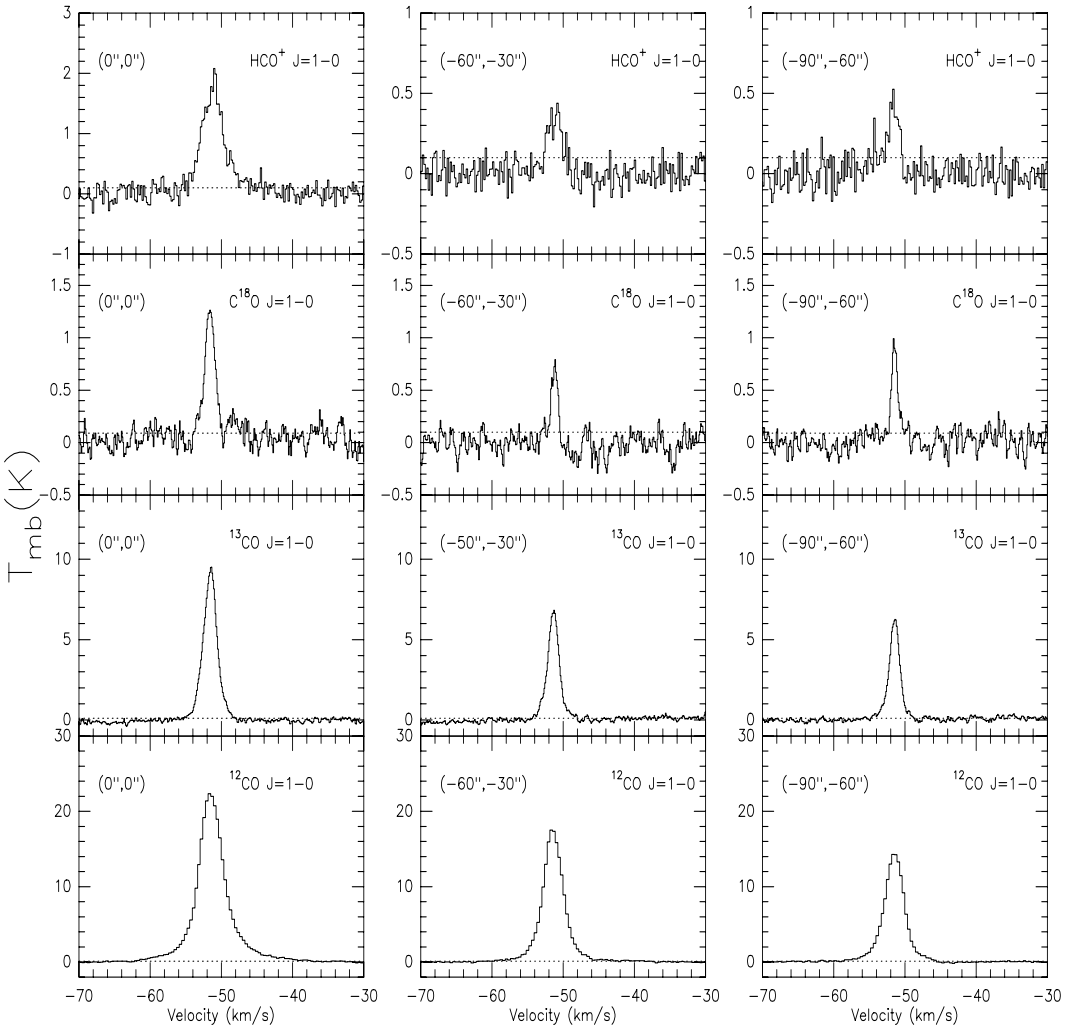

Fig. 2 *Left panel:* spectra at the $C^{18}O$ east peak. *Middle panel:* spectra at the conjunctive point of the two $C^{18}O$ cores. *Right panel:* spectra at the $C^{18}O$ west peak. The horizontal dotted line is the 1σ level of each line (Table 1).

From Figure 3, we see that both the molecular line and the dust emission peak are roughly coincident with the IRAS source. ^{13}CO and HCO^+ are dominant with a single core. ^{13}CO shows a small elongation. The $C^{18}O$ map clearly shows two cores (Core A and Core B), indicating that such an optically thin line traces the inner part of a molecular cloud compared to the other two lines. The center of Core A, with an angular extent of (70″, 60″), coincides with IRAS 22506+5944 and the MSX peak, indicating that they may be the same source. Core B has an offset of (100″, 60″) at the north-west of Core A. The size of Core A is slightly larger than Core B (70″, 60″). In order to show the kinematic relation between the two cores, we also give channel maps of the ^{13}CO $J = 1 - 0$ lines in Figure 4.

We derive the physical parameters of the cores, assuming LTE (local thermodynamic equilibrium) and with an abundance ratio $[H_2]/[^{12}CO] = 10^4$. Given a distance from the source to galactic center of $D_{GC} \sim 11.4$ kpc, we adopt an abundance ratio $[^{12}CO]/[C^{18}O] \simeq 707$ and $[^{12}CO]/[^{13}CO] \simeq 93$ estimated from the relationship $[^{16}O]/[^{18}O] = (58.8 \pm 11.8)D_{GC} + (37.1 \pm 82.6)$ and $[^{12}C]/[^{13}C] = (7.5 \pm 1.9)D_{GC} + (7.6 \pm 12.9)$ (Wilson & Rood 1994). Excitation temperature is calculated using Equation (1), assuming

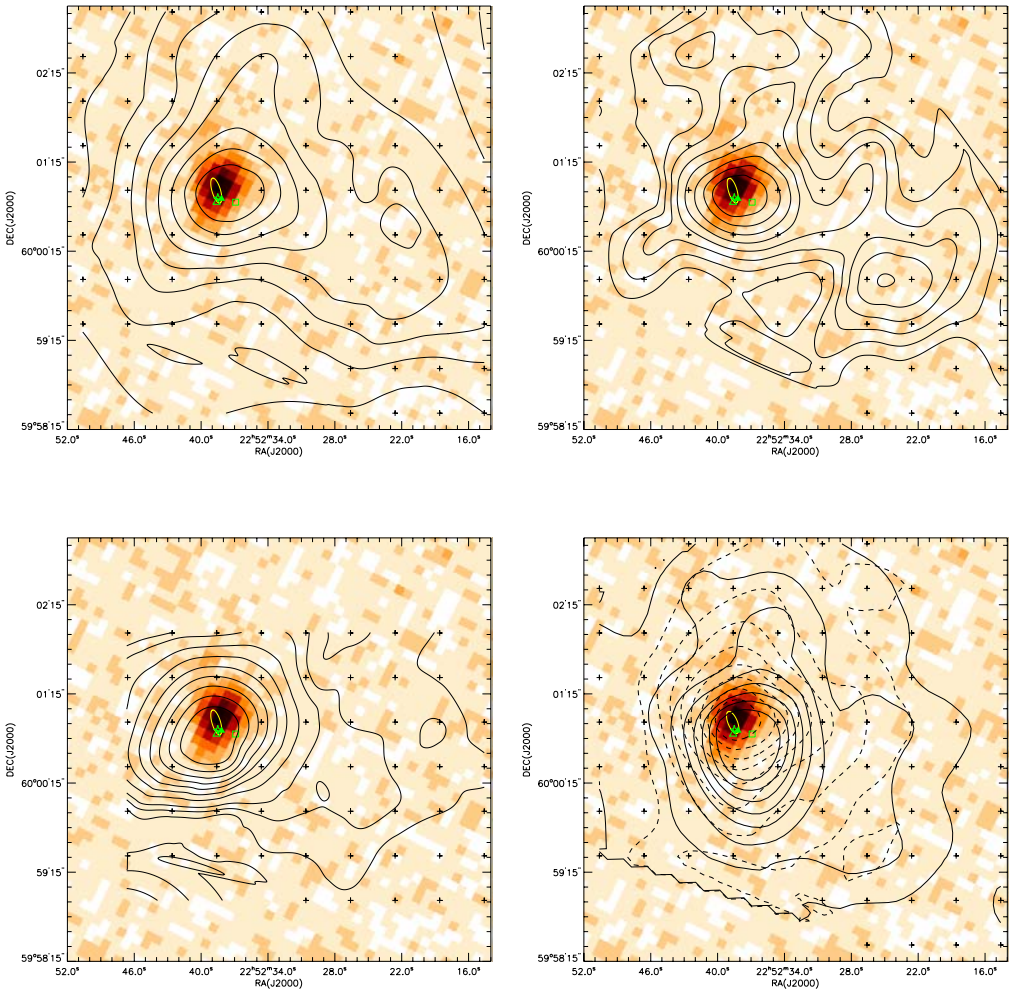

Fig. 3 *Upper left*: contour map of the total integrated ^{13}CO $J = 1 - 0$ line emission in the velocity range from –53.4 to –49.5 km s^{-1} overlain on an MSX *E* band 21 μm image. *Upper right*: contour map of the total integrated C^{18}O $J = 1 - 0$ line emission in the velocity range from –52.1 to –50.8 km s^{-1}. *Lower left*: contour map of the total integrated HCO$^+$ $J = 1 - 0$ line emission in the velocity range from –52.6 to –49.5 km s^{-1}. *Lower right*: contour map for the ^{12}CO $J = 1 - 0$ outflow. The blue wing (*solid line*) emission was integrated over –60 to –54 km s^{-1} and –49 to –42 km s^{-1} for the red wing (*dashed line*), respectively. Contour levels of the plots are all from 20% to 90% in steps of 10% of each peak emission with the exception of the HCO$^+$ $J = 1 - 0$ lines, whose contour levels are 10%, 15% and 20% to 90% in steps of 10%. 50% contour levels used to determine core sizes are plotted with thicker lines. The small crosses in the contour plots show the measured positions and the ellipses mark the IRAS error ellipse. The filled triangles denote the 3 mm continuum peak (Su et al. 2004). H_2O (Wooterloot & Walmsley 1986), SiO (Harju et al. 1998) and CH_3OH masers are indicated by open symbols of triangle, star and square, respectively.

that the ^{12}CO $J = 1 - 0$ lines are optically thick:

$$T_{\rm ex}^{*} = 5.532 \left\{ \ln \left[1 + \frac{5.532}{\left(T_R^{*}(^{12}{\rm CO}) + 0.819 \right)} \right] \right\}^{-1}, \quad (1)$$

^{13}CO and C^{18}O $J = 1 - 0$ line optical depths, τ, are estimated with the formulas below:

$$\tau(^{13}\mathrm{CO}) \approx -\ln\left[1 - \frac{T_R^*(^{13}\mathrm{CO})}{T_R^*(^{12}\mathrm{CO})}\right], \tag{2}$$

$$\tau(\mathrm{C}^{18}\mathrm{O}) \approx -\ln\left[1 - \frac{T_R^*(\mathrm{C}^{18}\mathrm{O})}{T_R^*(^{12}\mathrm{CO})}\right]. \tag{3}$$

^{13}CO and C^{18}O column densities are derived using Equation (4) (Kawamura et al. 1998) and Equation (5) (Sato et al. 1994). τ and $\Delta\nu$ are the optical depth and intrinsic line width:

$$N\left(^{13}\mathrm{CO}\right) = 2.42 \times 10^{14} \frac{T_{\mathrm{ex}}\tau(^{13}\mathrm{CO})\Delta\nu(^{13}\mathrm{CO})}{1 - \exp\left(-5.29/T_{\mathrm{ex}}\right)}\mathrm{cm}^{-2}, \tag{4}$$

$$N\left(\mathrm{C}^{18}\mathrm{O}\right) = 2.24 \times 10^{14} \frac{T_{\mathrm{ex}}\tau(\mathrm{C}^{18}\mathrm{O})\Delta\nu(\mathrm{C}^{18}\mathrm{O})}{1 - \exp\left(-5.27/T_{\mathrm{ex}}\right)}\mathrm{cm}^{-2}. \tag{5}$$

The nominal core size, l, is determined by de-convolving the telescope beam, using Equation (6):

$$l = D\left(A_{1/2} - \theta_{\mathrm{MB}}^2\right)^{1/2}, \tag{6}$$

where D is the distance (5.0 kpc), $A_{1/2}$ is the area within the contour at the half-integrated intensity of the peak and θ_{MB} is the main beam size (see Table 1).

Core masses are computed with Equation (7), where m is the mass of the hydrogen molecule, μ the ratio of total gas mass to hydrogen mass, $\mu \approx 1.36$ (Hildebrand 1983), $N_{\mathrm{H_2}}$ the column density of H_2 and l the de-convolved half power size defined above.

$$M_{\mathrm{LTE}} = \mu m N_{\mathrm{H_2}} l^2/4. \tag{7}$$

The derived physical parameters are tabulated in Table 3.

Table 3 Physical Parameters of Core A and Core B

Name	$\Delta\alpha$ (arcsec)	$\Delta\delta$ (arcsec)	l (pc)	Tex (K)	$\Delta\nu$ [a] (km s^{-1})	$N(^{13}\mathrm{CO})$ (cm^{-2})	$N(\mathrm{C}^{18}\mathrm{O})$ (cm^{-2})	$N(\mathrm{H_2})$ [b] (cm^{-2})	M_{LTE} $M_\odot$
Core A	90	70	0.9	26	1.5	2.7E+16	1.7E+15	2.7E+22	228
Core B	85	60	0.5	18	1.0	10.7E+15	7.5E+14	1.1E+22	35

[a]: $\Delta\nu$ has been corrected using $\frac{\Delta V_{\mathrm{line}}}{\Delta V_{\mathrm{true}}} = \sqrt{\frac{\ln[\tau/\ln 2/(1+e^{-\tau})]}{\ln 2}}$, considering line broadening due to optical depth.
[b]: H_2 column densities were derived using ^{13}CO column densities, assuming $[H_2]/[^{13}\mathrm{CO}] = 9.3\times10^5$.

3.2.2 Outflows

Molecular outflows are an important signature of the earlier stage of star formation. An outflow has been detected (Wu et al. 2005) using the ^{12}CO $J = 2 - 1$ line. A comparison of two different transitions will be helpful to our better understanding of the physical properties of outflows. In Figure 3, we present similar work with the ^{12}CO (1–0) line. The red and blue lobes largely overlap, while the IRAS source is located at the center of the outflow, which is probably the driving source of the outflow. The morphology of the ^{12}CO $J = 1 - 0$ outflow is similar to that of the ^{12}CO $J = 2 - 1$ outflow (Wu et al. 2005), but the former extends over a larger area than the latter, spreading from Core A to Core B.

The outflow parameters, except for the ^{12}CO column density which is derived from Snell et al. (1988), are estimated with the method of Beuther et al. (2002). We assume that the gas is in LTE and the line wings are optically-thin. The excitation temperature and $[H_2]/[^{12}\mathrm{CO}]$ abundance ratio adopted

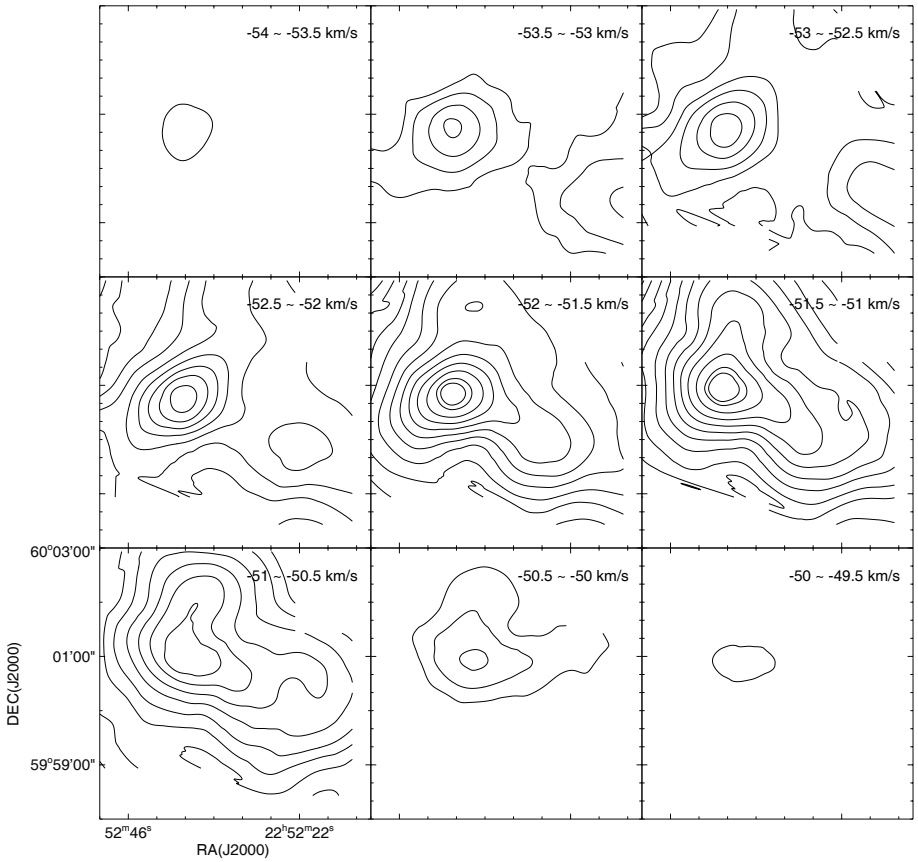

Fig. 4 Channel maps of ^{13}CO $J = 1 - 0$ lines with contour levels starting at 0.4 K km s^{-1} and separated by 0.3 K km s^{-1}.

Table 4 Outflow Properties

Component	$V_{\rm range}$ (km s^{-1})	Size[a] (pc)	$N(H_2)$ (cm^{-2})	Mass $M_\odot$	P ($M_\odot$ km s^{-1})	$E_{\rm k}$ (erg)
red lobe(L)	(–48.2 –44.0)	0.8	1.3E+20	5.3	72	9.6E+45
red lobe(H)	(–44.0 –38.0)	0.8	4.2E+19	2.1	29	3.8E+45
blue lobe(L)	(–54.7 –59.0)	1.0	1.0E+20	6.6	68	7.1E+45
blue lobe(H)	(–59.0 –62.0)	1.0	1.7E+19	1.0	11	1.1E+45
total	—	—-	—	15.0	180	2.2E+46

[a]: Sizes of lobes are computed using formula (6).

are the same as in Section 3.2.1. In order to better define the kinematics of the high gas, we divided the wings into low velocity and high velocity segments. The physical properties, including velocity range, size, column density, mass, momentum and kinetic energy, are summarized in Table 4.

Following the method of Beuther et al. (2002), we obtain the characteristic time scale, $t \approx 8.1\times\ 10^4$ yr, the mass loss rate, $\dot{M}_{\rm out} \approx 1.8 \times 10^{-4} M_\odot\,{\rm yr}^{-1}$; the mechanical force, $F_{\rm m} \approx 2.2 \times 10^{-3} M_\odot\,{\rm km\ s^{-1}\ yr^{-1}}$; and the mechanical luminosity, $L_{\rm m} \approx 2.2 L_\odot$. The mass and kinetic energy of the outflow are significantly larger than typical values from low-mass star-forming regions (Bontemps et al. 1996).

3.3 Evolutionary Scenario

HCO^+ usually traces the geometrically thick envelope of a core, while $C^{18}O$ is expected to trace the inner part of the core. The $C^{18}O$ map clearly shows two cores, Core A and Core B, which likely consist of two star-forming regions. Core A shows obvious star-forming evidences, such as strong middle and far infrared emission, masers and outflows, while Core B is only associated with some cold molecular lines, indicating that Core A and Core B are at different evolutionary stages; Core A is in the protostar core phase, while Core B is probably in the pre-stellar core phase. The mass of Core A is more than $200\,M_\odot$, while the IRAS source has a luminosity of $1.5 \times 10^4\,L_\odot$. According to the relation between mass and luminosity, $L \sim M^{3.5}$, the core mass is around one order of magnitude larger than that of the IRAS source. This indicates that there are other sources within the core, which are not detected due to the resolution limit of the employed telescope. With a rising steep spectrum, the IRAS colors imply that the source is deeply embedded in a dense molecular cloud. This IRAS source could be the exciting source of the H_2O, SiO and CH_3OH masers. Core B has a mass of about $35\,M_\odot$, which might form several low and/or medium mass stars in the future. The energetic outflow driven by IRAS 22506+5944 covers the whole region, including both Core A and Core B, and could greatly affect its surroundings and accelerate Core B to form stars. In summary, the whole region is a star-formation complex, in which stars at different evolutionary stages live in the same cluster and interact with each other.

4 SUMMARY

Our multi-line study reveals a star-formation complex around IRAS 22506+5944, in which a weak 6.7 GHz CH_3OH maser was detected. Multi-line maps reveal a two-core structure: Core A with a mass of $\sim 230\,M_\odot$ contains the IRAS source which is driving an energetic bipolar outflow, while Core B, significantly smaller than Core A, has a large offset from the IRAS source. The two cores are at different evolutionary stages. The energy released by the more evolved core (Core A) is influencing the relatively less evolved core (Core B) to accelerate its process in forming stars.

Acknowledgements We wish to thank all the staff at the Qinghai Station of the Purple Mountain Observatory for their assistance with our observations. This work was supported by the National Natural Science Foundation of China (Grant Nos. 10673024, 10733030, 10703010 and 10621303) and the National Basic Research Program of China-973 Program (2007CB815403).

References

Beuther, H., Schilke, P., Sridharan, T. K., Menten, K. M., et al. 2002, A&A, 383, 892
Bontemps, S., André, P., Terebey, S., & Cabrit, S. 1996, A&A, 311, 858
Breckenridge, S. M., & Kukolich, S. G. 1995, ApJ, 438, 504
Harju, J., Lehtinen, K., Booth, R. S., & Zinchenko, I. 1998, A&AS, 132, 211
Harju, J., Walmsley, C. M., & Wouterloot, J. G. A. 1993, A&AS, 98, 51
Hildebrand, R. H. 1983, QJRAS, 24, 267
Kawamura, A., Onishi, T., Yonekura, Y., et al. 1998, ApJS, 117, 387
Minier, V., Ellingsen, S. P., Norris, R. P., & Booth, R. S. 2003, A&A, 403, 1095
Molinari, S., Brand, J., Cesaroni, R., Palla, F., et al. 1998, A&A, 336, 339
Ott, M., Witzel, A., Quirrenbach, A., et al. 1994, A&A, 284, 331
Sato, F., Mizuno, A., Nagahama, T., et al. 1994, ApJ, 435, 279
Snell, R. L., Huang, Y.-L., Dickman, R. L., & Claussen, M. J. 1988, ApJ, 325, 853
Su, Y.-N., Zhang, Q.-Z., & Lim, J. 2004, ApJ, 604, 258
Szymczak, M., Hrynek, G., & Kus, A. J. 2000, A&AS, 143, 269
Wilson, T. L., & Rood, R. 1994, ARA&A, 32, 191
Wouterloot, J. G. A., & Walmsley, C. M. 1986, A&A, 168, 237
Wu, Y., Zhang, Q.-Z., Chen, H., Yang, C., et al. 2005, AJ, 129, 330
Xu, Y., Shen, Z.-Q., Yang, J., Zheng, X. W., et al. 2006, AJ, 132, 20
Xu, Y., Zheng, X.-W., & Jiang, D.-R. 2003, ChJAA (Chin. J. Astron. Astrophys.), 3, 49